Reprint from

PLASMA PHYSICS AND CONTROLLED NUCLEAR FUSION RESEARCH 1990

PROCEEDINGS OF THE
THIRTEENTH INTERNATIONAL CONFERENCE ON PLASMA PHYSICS
AND CONTROLLED NUCLEAR FUSION RESEARCH
HELD BY THE
INTERNATIONAL ATOMIC ENERGY AGENCY
IN WASHINGTON, D.C., 1-6 OCTOBER 1990

In three volumes

VOLUME 3

INTERNATIONAL ATOMIC ENERGY AGENCY
VIENNA, 1991

INERTIAL CONFINEMENT FUSION RESEARCH AT THE SERC CENTRAL LASER FACILITY, UNITED KINGDOM

O. WILLI, T. AFSHAR-RAD, A.R. BELL, M. DESSELBERGER, J. EDWARDS, L. GIZZI, G. RICKARD, R. TOWN, I. WILLIAMS
Imperial College of Science, Technology and Medicine,
London

M. LAMB, M. SAVAGE
The Queen's University of Belfast,
Belfast

P. FEWS
University of Bristol,
Bristol

C. DANSON, S. ROSE
Rutherford Appleton Laboratory,
Chilton, Didcot

United Kingdom

Presented by M.G. Haines

Abstract

INERTIAL CONFINEMENT FUSION RESEARCH AT THE SERC CENTRAL LASER FACILITY, UNITED KINGDOM.

The paper summarizes a research programme of experimental and theoretical work carried out by several University groups in the United Kingdom and by the staff of the laser division of the Rutherford Appleton Laboratory. A number of areas have been covered, resulting in several novel contributions relevant to inertial confinement fusion. The main effort of recent research concentrated on studies with improved laser illumination uniformity generated by Random Phase Plate (RPP) Arrays and Induced Spatial Incoherence (ISI) techniques or by a combination of both. In particular, beam plasma and Rayleigh–Taylor instabilities have been investigated on targets irradiated with incoherent laser light. In addition, computational work was carried out to study the effects of incoherent irradiation. For example, thermal transport processes were investigated with a Fokker–Planck code. Further, thermal instabilities of the overdense plasma blow-off were studied by using novel XUV probing techniques. The transport of soft x-ray radiation through thin foil targets was investigated both experimentally and computationally. Three-dimensional hydrodynamic simulations were carried out to study the Rayleigh–Taylor instability in spherical geometry.

INTRODUCTION

This paper includes experimental and theoretical work relevant to inertial confinement fusion which was carried out in connection with the high power laser programme of the SERC Central Laser Facility, undertaken by various university groups and inhouse staff. The main effort of recent research concentrated on studies with improved laser illumination uniformity generated by Random Phase Plate (RPP) Arrays and Induced Spatial Incoherence (ISI) techniques.

The suppression of instabilities including laser beam filamentation, stimulated Raman and Brillouin scattering has been studied in large underdense plasmas with laser beams smoothed by RPP Arrays or ISI. Millimetre-sized cylindrical underdense high temperature plasmas were produced by irradiating thin foil targets with a number of laser beams in a line focus geometry. A separate laser beam interacted axially with the preformed plasma. Significant reductions in both the SRS and SBS levels were seen for both smoothing methods. In addition, preliminary results indicate that the ISI interaction pulse may self-focus in the preformed plasma.

Fokker-Planck simulations have been carried out to investigate the effects of ISI and RPP on electron thermal transport and ablation pressure uniformity. A new effect, 'thermal inertia smoothing', has been identified resulting in a smoother Fokker-Planck temporal and spatial variation of the ablation pressure than that for Spitzer for the same applied time varying laser intensity.

The transport of soft x-ray radiation through thin foil targets has been studied using time resolved XUV spectroscopy. An intense source of soft x-ray radiation was produced by overcoating the front side of the target with gold and irradiating it with laser light smoothed by RPP. The experimental observations clearly showed that the soft x-ray spectrum emitted from the rear surface of the target was distinctly different from the one incident onto the front of the target. The experimental results were simulated with a multi-group S2 radiation transport code which was coupled to a one-dimensional hydrodynamics code. The material opacity was determined using an average-atom screened-hydrogenic model in local thermodynamic equilibrium. A good global agreement between the experimental observations and the simulations was obtained.

Growth rates of the Rayleigh-Taylor instability were measured in thin foil targets with imposed sinusoidal modulations irradiated by optically smoothed laser beams. A hybrid optical smoothing scheme utilising ISI and RPP was used. The enhancement in the modulation depth during acceleration was observed with time resolved transmission radiography using a soft x-ray backlighting source. The wavenumber dependence and nonlinearity of the RT growth were investigated by using a range of modulation periodicities and depths. The measurements were compared with 2-D hydrocode simulations. The RT instability was also studied by using α-particle backlighting techniques. The α-particles were generated in laser driven implosion.

Detailed modelling of RT instability was carried out with a 3−D Eulerian fluid code. In particular at the later stages, the imploding shell is subject to RT instabilities and convergent amplification of non−uniformity, both of which reduce the density of the final core.

STUDY OF INSTABILITIES IN LONG SCALELENGTH PLASMAS WITH AND WITHOUT LASER BEAM SMOOTHING TECHNIQUES

The interaction of intense laser light with large underdense plasmas is of great interest for inertial confinement fusion since fusion pellets will be surrounded by large plasma coronas. Under these conditions various parametric instabilities such as Stimulated Brillouin Scattering (SBS), Stimulated Raman Scattering (SRS) and laser beam filamentation may be very effective resulting in the reduction of laser plasma coupling, in the production of high energy electrons and in the nonuniform heating of the plasma corona. To simulate fusion conditions plasmas with scalelengths of about one millimetre were recently produced by focusing four green laser beams of the Rutherford Appleton Laboratory high power laser system onto thin foil targets in a line focus configuration. A delayed green laser beam was focused axially into the preformed underdense plasma with an electron temperature and density of about 0.5 keV and 0.1 n_c respectively. Significant levels of SRS and SBS were seen [1] and laser beam filamentation and whole beam self−focusing was clearly observed [2,3]. When the incident laser beam was smoothed either by Random Phase Plate Arrays (RPPA) or Induced Spatial Incoherence (ISI) a significant reduction in the absolute levels and the virtual suppression of filamentation was seen [4,5].

In this paper experimental results of a recent investigation are reported. The preformed plasma was again formed by a line focus configuration using four heating beams. However the heating beams were also smoothed by ISI in contrast to previous measurements in order to produce a more uniform preformed plasma. Either an ISI smoothed infrared (1.05 μm) laser beam or a broadband beam delayed by 2.2 ns was focused axially into the plasma. An extensive set of diagnostics was used to investigate the plasma conditions of the preformed plasma and the nonlinear interaction of the laser beam with the plasma.

The model plasma was generated by irradiating a thin aluminium foil target (700 nm thick, 0.7 mm long, 300 μm wide) which was overcoated on a 100 nm thick formvar substrate. Two pairs of opposing green laser beams smoothed by Induced Spatial Incoherence were superimposed in a line focus configuration as heating beams to form the plasma. Typical irradiances of 10^{14} Wcm^{-2} were used. A separate infrared laser beam typically delayed by 2.2 ns was used to interact with this plasma along its longitudinal axis. Measurements were made with the broadband beam ($\Delta\omega/\omega \simeq 0.1\%$) or with an ISI laser beam [6]. At the time of interaction the nominal electron density was about 0.3 n_c (n_c is critical density for the infrared laser light) and the electron temperature was about 500 eV of the preformed plasma.

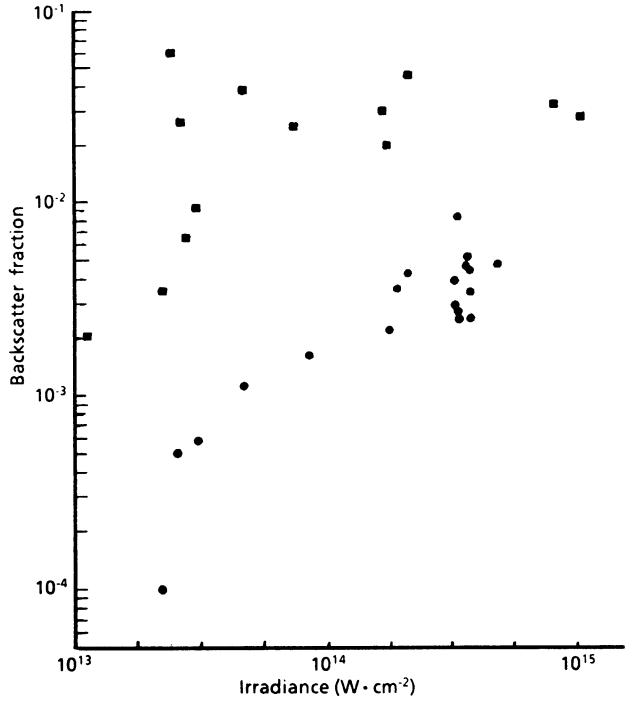

FIG. 1. Variation of SBS backscatter fraction with average irradiance for an ISI (illustrated by the solid circles) and a broadband (squares) interaction beam.

The uniformity of the preformed plasma was investigated transversely to the exploding foil target by using optical Moire deflectometry techniques with a probe wavelength of 350 nm. The density profile was measured interferometrically with 350 nm probe beam propagating along the axis of the preformed plasma. The electron temperature of the plasma was obtained from time resolved x-ray streak spectroscopy. The backscattered Brillouin signal generated by the interaction beam was imaged out via the incident focusing lens onto a calibrated photodiode. In addition, time resolved SBS spectra were recorded with an S1 optical streak camera. A four frame x-ray pinhole camera with a gating time of about 150 ps was used to observe the x-ray emission of the preformed plasma and of the interaction beam.

Figure 1 shows the absolute levels of SBS backscattering for the ISI and broadband interaction beams as a function of the incident irradiance. The focal spot of the interaction beam was 140 μm in diameter and was kept constant for all the data shots. For the broadband laser beam a threshold at an irradiance of about 3×10^{13} Wcm^{-2} is observed with a saturation level between 2 to 6% of the incident laser energy. For the ISI interaction beam an exponential behaviour is seen with an average SBS value of 0.5% at an

irradiance of $7x10^{14}$ Wcm^{-2}. The SBS backscattering levels are significantly higher than observed in a previous experiment [4,5] in which a green interaction beam was used, the plasma was less uniform and the electron density was lower (by about a factor of 3) during interaction. However similar SBS levels are seen in the present experiment when thinner targets 500 nm in thickness are used resulting in a similar electron density as used previously. The estimated electron density is consistent with backscattered Simulated Raman Scattering (SRS) which was detected by diodes filtered with narrowband interference filters. For the 700nm targets virtually no SRS backscatter is observed. On the other hand, clear SRS signals (at a wavelength of about 1.5 μm) are seen with the 500 nm. The significant larger SBS level observed in the present experiment may be a result of the improved uniformity of the preformed plasma.

For some of the data shots the first experimental evidence of whole beam self-focusing of an ISI laser beam was obtained. Gated x-ray pinhole camera images with a framing time of 120 ps showed a channel like structure with a diameter of about 40 μm. The pinhole camera was filtered with 3 μm of aluminium. Fig. 2 shows a series of x-ray images. The irradiance of the interaction pulse was $2.3x10^{14}$ Wcm^{-2} with a pulse duration of 550 ps (FWHM). Optical probing images taken simultaneously with the x-ray records were consistent with the x-ray images. In addition, the SBS backscattered signal increased by a factor of 8 for these shots compared to the data taken with similar irradiances where no self-focusing was observed.

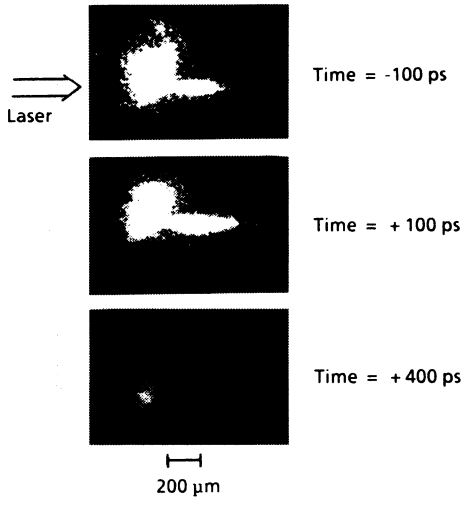

FIG. 2. Time resolved x-ray pinhole images recorded on the same shot showing whole beam self-focusing of an ISI pulse which propagates through a preformed plasma. The timing of the frames is −100 ps (100 ps in front of the pulse peak), +100 ps and +400 ps, respectively.

FOKKER-PLANCK SIMULATIONS OF PLASMAS IRRADIATED BY AN INCOHERENT LASER

A Fokker-Planck code was used to examine the effects of ISI on the heat flow. The simulations are compared to calculations carried out by a Spitzer code which uses the classical Spitzer-Harm thermal conductivity with a harmonic flux limiter. To mimic the fluctuations inherent in ISI, an oscillating laser intensity in 1-D is imposed on a plasma with an initial density scalelength of 3 μm and a maximum electron density of $9\text{x}10^{22}$ cm^{-3},

$$I(t) = I_0(1+\cos(\pi t/\tau))\exp(-(t-t_0)^2/2\sigma^2)$$

with $I_0 = 5\text{x}10^{14}$ Wcm^{-2}, $t_0 = 100$ ps, $\sigma = 45$ ps, $\lambda_{laser} = 0.25$ μm. The target is fully ionised and $Z = 4$.

The Spitzer simulations show a greater temporal fluctuation in ablation pressure than the FP results. In 2-D, an ISI-type intensity profile is used, consisting of multiwavelength time-dependent spatial perturbations in the transverse direction. A coherence time of 1 ps is imposed. The FP always has a smaller P_{max}/P_{min} than that predicted by Spitzer. $P_{max}(P_{min})$ is the maximum(minimum) pressure along the ablation front.

Nonlocal effects reduce the heat flow from the absorption to ablation regions, so that changes at the absorption surface are not communicated to the ablation surface as strongly with nonlocal transport as with Spitzer. We conclude that $\triangle P/P_{abl}$ for a given $\triangle I/I$ with an incoherent laser is smaller than would be predicted by fluid codes using Spitzer conductivity.

INVESTIGATIONS OF THERMAL INSTABILITIES IN OVERDENSE PLASMAS USING XUV PROBING TECHNIQUES

After the first experimental evidence of jet formation in the plasma corona of laser irradiated targets was provided using optical probing techniques [7,8], considerable theoretical interest was stimulated. A number of mechanisms for the production of the jet-like structures have been proposed in theoretical studies. For a review see Ref. 9.

Until now, no experiment has however clearly identified the responsible mechanism, nor has any evidence been obtained of the effect of these instabilities on the ablation rate or on thermal smoothing. Of particular importance to the ICF programme is the question of whether the jets exist only in the subcritical region (all experimental work until now has provided information only about the subcritical region) or whether they extend into the supercritical region, where their effects are potentially far more detrimental for implosion symmetry. It is of paramount importance to investigate the superdense region for the occurrence of these instabilities with good spatial and temporal resolution.

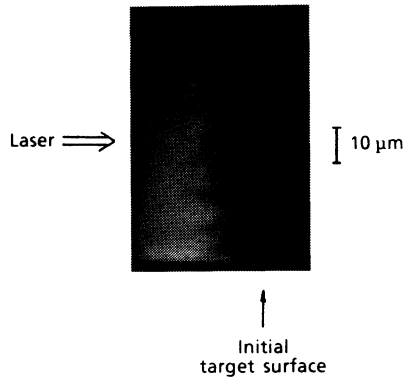

FIG. 3. XUV image of laser heated gold wire target showing a jet-like structure in the overdense plasma.

A novel experimental technique based on only recently available multilayered mirror technology for use in the XUV spectral region has been developed. As it is well known, optical probing is limited to the sampling of relatively low density regions $n_e < n_c$, since the optical rays are refracted out of the imaging optics by the steep plasma density gradients. Shorter wavelengths are refracted less and simulations show that XUV probe wavelengths approximately of about 100 Å will in combination with imaging effectively probe the conduction region up to several times critical density.

The imaging system consisted of a spherical mulitilayered mirror operating at a wavelength of 130 Å with a bandwidth of 20 Å. An XUV source was generated by irradiating a gold target at an intensity of about 10^{14} Wcm^{-2}. The image was recorded with a microchannel plate intensifier. The overall magnification of the system was about 70x. The spatial resolution was measured by using a zone plate as an object. It was found to be about 0.8 μm and was limited by the spatial resolution of the microchannel plate. The temporal resolution was 120 ps which was the gating time of the microchannel plate detector. Fig. 3 shows an XUV shadowgram recorded on a laser irradiated gold coated wire target 10 μm in diameter. The irradiance on target was about 10^{13} Wcm^{-2}. The image was recorded 2.4 ns after the heating pulse. Jetting with a spatial scalelength of about 10 μm is clearly observed very close to the target surface.

MEASUREMENT AND ANALYSIS OF RADIATION TRANSPORT IN LASER IRRADIATED TARGETS

Thin foil plastic targets 0.1 to 5 μm thick overcoated with 100 nm of gold on the front side were irradiated with a single green laser pulse 700 ps in duration. The laser beam was focused onto target with an f/2.5 aspheric lens producing an irradiance between 1 to $5x10^{14}$ Wcm^{-2} at the target

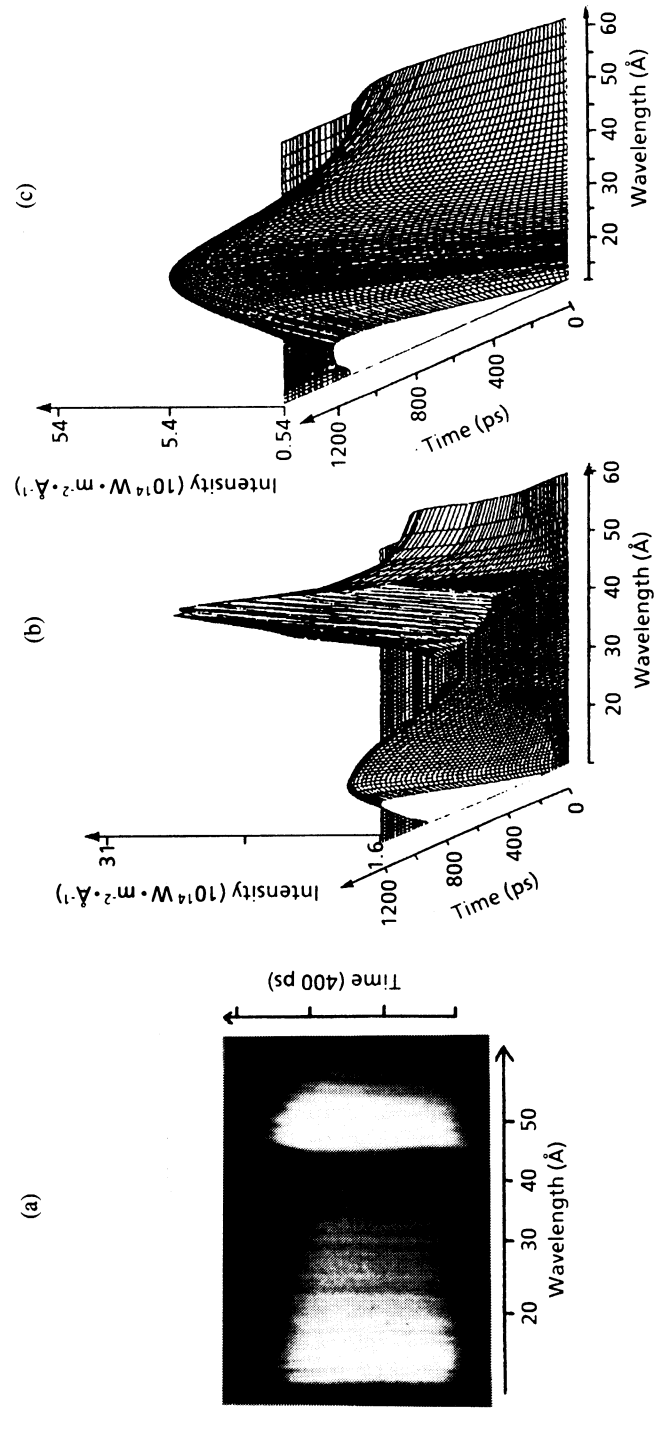

FIG. 4. (a) Experimental and (b) predicted spectra from the rear of a 5 μm CH target coated with 0.1 μm gold; (c) is the spectrum used in the simulations which is incident on the CH target.

surface. The focal spot size was measured with an x-ray pinhole camera filtered for the 1.5 keV energy range and was typically 400 μm (FWHM) in diameter. The soft x-ray radiation transported through the rear side of the thin foil targets was time resolved using a grazing incidence flat field spectrometer coupled to an XUV streak camera. The temporal and spectral resolution was 50 ps and 0.2 A respectively. The soft x-ray radiation was reflected into the spectrograph by a highly polished silica mirror set at a grazing incidence angle of 2.5 degrees acting as a high frequency cut off filter for radiation above approximately 1 keV.

Numerical simulations were carried out for a 5 μm target using a multi-group radiation transport model coupled to the 1-D Lagrangian hydrodynamics code MEDUSA. Because the radiation field is not isotropic, the model distinguishes between inwardly and outwardly moving photons. Group averaged Planck mean opacities are calculated at the material temperature, in line with the hydrodynamics using an average-atom screened-hydrogenic approximation in LTE, based on the model XSN. Only bound-free and free-free transitions are considered in the model. The behaviour of the laser irradiated thin gold layer was not calculated in the code because of the marked non-LTE behaviour of the x-ray emitting region of the gold plasma which could not be accurately calculated by our LTE model.

Small inaccuracies in the gold spectral emission do not cause any serious errors in the material heating. Simulations were carried out with and without the inclusion of M, N and O emission bands. No significant differences in the overall predicted results were seen. T_{RMAX} was estimated to be 115 eV from absolute measurements which were taken under similar experimental conditions. This corresponds to an overall laser to x-ray conversion efficiency of approximately 12% towards the rear which is consistent with spectra taken on ultra thin 0.1 μm plastic substrates.

Figure 4 shows a time resolved x-ray spectrum in the 15 to 70 A spectral wavelength range of the radiation transported through the rear of a 5 μm thick plastic foil target which was overcoated with 0.1 μm of gold on the surface facing the laser beam. The gold layer was irradiated at an intensity of 1.5×10^{14} Wcm^{-2}. Note the clear presence of a sharp edge-like feature at around 45 A in the XUV spectrum and the apparent early turn on of radiation on the longer wavelength side. In addition, away from the edge, the emission of radiation towards longer wavelength appears to be progressively retarded with respect to that at shorter wavelength. Finally, the edge appears to move gradually towards higher energies later in time as the foil becomes heated. The maximum shift of this feature is measured to be 0.9 ∓ 0.2 A or 5.5 ∓ 1.2 eV. For comparison a 3-D plot of the predicted intensity of radiation in units of $Wm^{-2}A^{-1}$ into 2π str transported through a 5 μm plastic foil target as a function of time and wavelength for T_{MAX} = 115 eV. In common with the experiment, the simulations show a clear edge which is due to the carbon K-edge, the early turn on of radiation just below (in energy) and well above the edge, progressively retarded emission of radiation towards longer wavelength away from the edge and a gradual shift in the edge position as the foil is heated.

The position of the edge feature in the experimental data is at approximately 45 A which corresponds to the cold carbon K-edge position. Maximum shifts of about 1 A were seen during the heating phase. In contrast, much larger shifts of the carbon K-edge positions are predicted in the simulations depending on the temperature of the heated material. For example, a shift of more than 10 A towards shorter wavelength is seen for a peak radiation temperature of 115 eV.

It is suggested that the small shift in the edge position in the experiment may be due to filling in of the photoabsorption below the shifted K-edge by line absorption [10]. The edge in figure 4 would then correspond to the side of a strong carbon absorption line. This explanation is supported by the plasma conditions predicted to exist in the foil. At the peak of the pulse, the density in the target is approximately constant at 0.1 gcm^{-3} and the temperature varies from approximately 100 eV near the front of the foil to just below 30 eV at the rear. The average degree of ionization calculated by the model decreases from just over 5 at the front of the target to approximately 3.5 at the rear. Therefore, a large number of bound-bound transitions will exist in the soft x-ray energy region due to an abundance of several different ionic species in the plasma.

STUDY OF RAYLEIGH - TAYLOR INSTABILITY USING X-RAY BACKLIGHTING TECHNIQUES

The Rayleigh-Taylor instability occurs in any accelerating fluid system in which the density and pressure gradients are of opposite sign. In the case of ICF experiments, the hot, low density ablating plasma accelerates a cooler, more dense part of the target and is thus succeptible to the RT instability. In an ICF implosion small imperfections in the target manufacture or intensity nonuniformities present in the laser irradiation may initiate RT growth sufficient to disrupt the target symmetry to an unacceptable degree.

Six frequency doubled green (0.53μm) beams arranged in a hexagonal cluster with a cone angle of 13 degrees were focused onto thin foil targets with f/10 lenses. The six superimposed beams generated a smooth, flat-topped spatial intensity profile providing uniform acceleration across the target surface. The total energy delivered on target was approximately 250 Joules with a pulse duration of 1.76 ns (FWHM) resulting in an incident irradiance of about 1.5×10^{14} Wcm^{-2}. This was kept constant throughout the experiment to allow direct comparison of the results for different target specifications. The laser beams were smoothed by a hybrid scheme consisting of Induced Spatial Incoherence (ISI) and Random Phase Plate (RPP) arrays. The ISI was generated using a broad-band oscillator ($\Delta\omega/\omega$=0.1%) and a 6x6 echelon to produce 36 independent beamlets. The RPP's were placed immediately in front of each of the six focusing lenses. In addition to profile smoothing, the RPP's have the effect of increasing the far-field focal spot size to the large (approx. 335 μm) diameter. A x-ray pinhole camera, filtered for an x-ray energy band between 0.84 keV and 1.63 keV, was used to monitor the uniformity of the focal spot produced by the drive beams.

Intensity variations of about 1% (calculated with a 2-D weighted averaging procedure) were seen over a spatial wavelength of 10μm. The far field focal spot distribution was calculated using an interference code. This showed close agreement to the experimentally determined profile structure and uniformity.

The targets consisted of low density (0.9g/cm^3) (CH_2) plastic approximately 16μm thick with sinusoidal modulations of periodicity 30μm, 50μm, 70μm and 100μm. Modulation depths between 1.8μm and 4.6μm were investigated, with the modulations always facing the drive beams. The accelerated targets were backlit with a Mg backlighter source which was generated by a separate green laser beam 2.5 ns in duration. The transmitted fraction of the x-rays produced by the backlighter source was imaged onto a streak camera by means of a pinhole 17 μm in diameter resulting in an overall spatial resolution of 21 μm. The image was filtered for a spectral wavelength window between 0.84 and 1.63 keV containing the magnesium Heα and Lyα transitions. The backlighter spectrum was measured using a time-integrated crystal spectrometer with filtering identical to that used in front of the streak camera. From this the relative contribution to the image intensity at each wavelength in the backlighter could be determined. Control experiments with only the drive irradiation (to determine the contribution to the image caused by self-emission from the target) and with backlighter illumination only were conducted. In addition to the transmission radiographs, streaked edge-on radiographs were recorded to obtain the target acceleration.

Computer simulations of the experiment were performed using the 2D Eulerian hydrodynamics code POLLUX which has been extensively tested under various conditions. The code was modified to incorporate the sinusoidal target surface modulations and matched to the experimental conditions by varying the absorbed irradiance until the inertial motion measured in the experiment was reproduced in the simulations. The absorbed intensity was chosen as the variable parameter, since it is the least well-characterised experimental quantity due to the effects of lateral energy transport. It was found that approximately 50% of the energy was absorbed and reproduced the experimentally determined inertial motion. This value is comparable to previous measurements under similar conditions.

From the transmission radiographs the ripple amplitude growth rates were determined by microdensitometry of the streak records to give quantitative measures of the observed X-ray contrast levels at different times. Both the initial modulation depth and the instability growth rate were then deduced from exponential curves fitted to the data [11]. The growth rates measured in this way are plotted in figure 5 as fractions of their classically predicted values, the errors representing the spread of the amplitude of modulation evident at late times. The measured initial (t=0) modulation depth were convolved with the modulation transfer function (MTF) of the imaging system and compared to the known initial modulation depths (accurately measured by microscopy before the experiment). No significant discrepancy was found (error $< 0.4\mu$m). Further, no growth rate analysis was carried out during the initial period in which the shock passes through

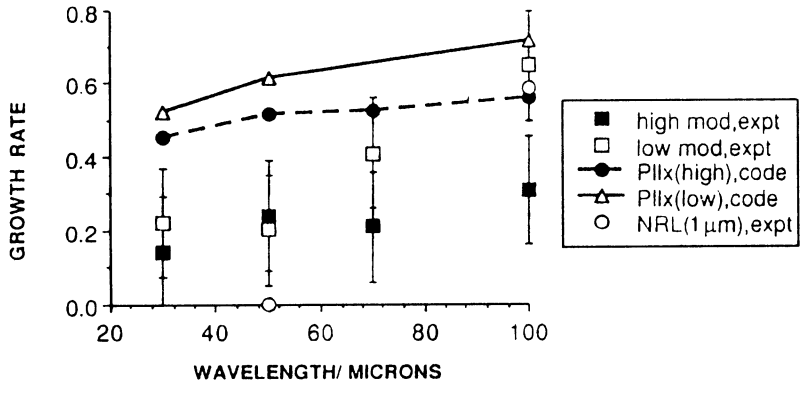

FIG. 5. Measured RT growth rates presented as a fraction of the classical growth rate $(kg)^{1/2}$, where k is the modulation wavenumber and g is the acceleration for both high (4.5 μm) and low (2.6 μm for 30 μm and 50 μm periodicity; 1.8 μm for 70 μm and 100 μm periodicity) modulation depth targets. Also shown are POLLUX results for 1.8 μm (low) and 4.5 μm (high) modulation depth targets and experimental results from Ref. [12], where the error bars are omitted for clarity.

the target. In this time, the growth is not due to the RT instability but due to the shock driven Richtmeyer–Meshkov instability.

The most striking result from figure 5 is that the 50μm periodicity targets clearly exhibited growth, where a previous experiment also utilising ISI (under low irradiance conditions ≃ $5x10^{12}$ Wcm^{-2}) [12] found none. The authors ascribed the result partially to the ISI irradiation and predicted with hydrodynamic code simulations that the ISI system is expected to delay the onset of growth.

Also plotted in figure 5 are the measured growth rates of the NRL experiment [12] and those predicted by the POLLUX simulations (for both high and low modulation depths). Several points arise. Firstly, the qualitative wavelength dependence of the observed growth rates is in fair agreement with the dependence predicted by the simulations; growth was observed at all modulation periodicities including 50μm. Secondly, the growth rates predicted by the simulations are (except for two points) outside the error bars and greater than the observed rates. This may not be purely due to the nonlinearity of the growth, but may in part be due to radiation transport effects not included in the modelling. These would, in principle, reduce the growth rate. The excitation of higher order modes also reduces the growth rate of the fundamental. To investigate the extent of such higher–order contributions to the growth of the instability, the X–ray radiographs were spectrally analysed with a Fourier decomposition package. It was found that small amplitude higher order modes are clearly present at late times (≃1.6ns after the start of the laser drive pulse) for 100μm modulation periodicity targets. Such higher harmonic modes were not clearly observed in the case

of the 50μm targets, where only the fundamental mode was found to have a significant Fourier component (for the case of 30μm targets, the resolution of the imaging system was insufficient to detect higher harmonic growth).

STUDY OF RAYLEIGH-TAYLOR INSTABILITY BY ALPHA PARTICLE BACKLIGHTING

Experiments have been performed to investigate the Rayleigh–Taylor instability in accelerated planar foils by an α–particle backlighting technique. In this technique, an α–particle source from a DT implosion produces a bright pulse of particles which are used to shadow a separately driven foil. Each α–particle loses range, determined by the local thickness of the foil at the time of passage of the particle. Since both the position and range of each particle are individually determined, any variation of thickness, even on a sub–micron spatial scale, will be recorded. In addition, a shadow image of the driven foil will be produced with a spatial resolution which is only limited by the source size and multiple Coulomb scattering in the plasma.

Alpha particles generated by the implosion travel through the laser accelerated foil target to a CR–39 detector. The system is entirely co–linear since the CR–39 is placed over the focusing lens. 3–D images are obtained with two spatial and one thickness dimension.

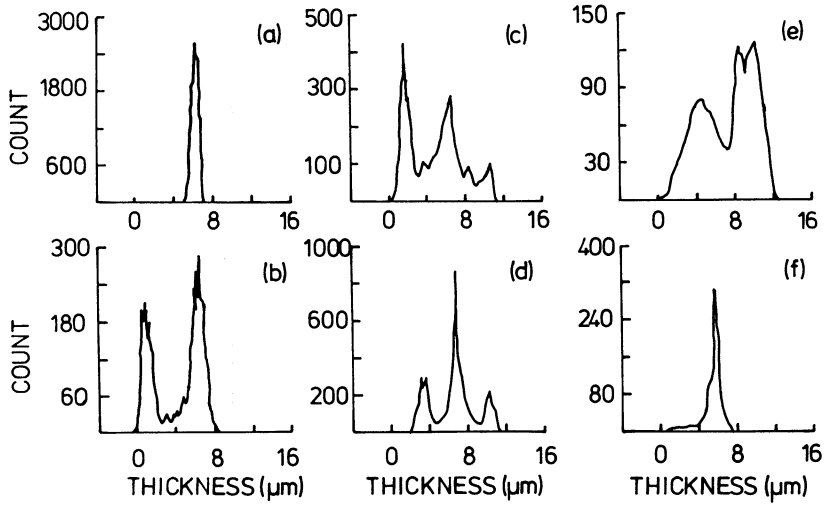

FIG. 6. Alpha particle spectra for (a) an undriven planar foil, (b) an undriven foil with deep modulations producing two separated peaks, (c) a foil with 1 μm seed probed at 1.0 ns, (d) as for (c) but probed at 0.5 ns, (e) a driven planar foil but probed at 2.0 ns, (f) a driven planar foil, probed at 2.0 ns but irradiated with RPP illumination.

Figure 6 shows some typical spectra. a) is obtained from an undriven planar foil target. b) is an undriven foil with 6 μm deep modulations producing two separate peaks. The width of these peaks is determined by the target thickness over the region sampled, and by limitation of the unfolding technique caused by the source width. c) is a foil with 1 μm seed probed at 1.0 ns. d) is as for c) but probed at 0.5 ns. e) is a planar foil but probed at 2 ns. The driven planar foils do not show a peak at zero thickness and reach the same induced modulaton at a later time as the seeded foils. f) is a driven planar foil, probed at 2.0 ns as in e), with the same intensity, but with RPP illumination. In contrast, this plot shows no increased modulation. There is, however, a small tail to the left of the peak, which is a feature not seen on the undriven foils. These may indicate some small residual spikes in the RPP focal spots.

These results may be interpreted that both unsmoothed laser beams and foil seeding have a significant effect on inducing mass modulations in the foils. It will be necessary to use smooth beams incident on modulated foils to observe the Rayleigh-Taylor instability.

THREE - DIMENSIONAL HYDRODYNAMIC SIMULATIONS OF LASER DRIVEN IMPLOSIONS

An important issue facing ICF is the implosion symmetry. A typical ICF compression can be characterised as passing through three phases: acceleration, coasting and deceleration. Initially the shell is accelerated inwards, defects in target manufacture or non-uniform laser irradiation can seed the Rayleigh-Taylor instability which grows on the outer, ablation surface. When the shell reaches maximum velocity it coasts inwards with little acceleration. Although not unstable the large spherical convergence can further distort the shell. As the pressure inside the filler gas increases so the shell is decelerated and finally brought to rest. In this final stage the shell is again unstable, but this time on the inner fuel-shell interface. Maximum density and temperature can only be achieved if the shell converges accurately towards the centre.

Previous simulations have concentrated on the initial acceleration phase. The ablation dynamics have been found to play a crucial role in the reduction of the observed RT growth rate to approximately one half the classical value. Full implosion simulations have been performed in 2-D using R-Z geometry. However 2-D simulations impose an unrealistic initial perturbation on the target and, unless a hemisphere is modelled, the boundary conditions would be incorrect.

Simulations have been carried out on the coasting and deceleration phase using PLATO. This is a fully 3-D hydrodynamics code with a fixed Eulerian grid. The time dependent equations of mass, momentum and total energy are integrated numerically. The fluid equations are closed using an ideal equation of state. Currently thermal conduction and laser energy deposition are not included.

At present the symmetry imposed on the target by the 12 laser beams are simulated. The point of intersection of the centre of each laser beam with the target surface defines the symmetry of the target. These points form the vertices of 20 equilateral triangles on the surface. Since the triangles are equilateral the sides can be bisected and 6 smaller triangles can be formed for each equilateral one. Hence the smallest self–similar component is 1/120th of the sphere. This is the computational grid that was used in all the simulations.

Since PLATO does not have any laser energy deposition all the simulations were initialised in the coasting phase. To study the coasting phase a 7 μm thick plastic shell was assumed to be coasting inwards with a velocity of $2x10^7$ cm/s at an initial inner shell radius R of 174 μm. The filler gas used was DT at a density of $1.05x10^{-2}$ g/cm^3 at a pressure of 100 bar. To prevent a transmitted shock travelling in front of the shell a radial velocity proportional to the radius was used in the filler gas.

When the pressure inside the filler gas is sufficiently large the shell starts to decelerate. The shell is now RT unstable. It is assumed that the shell's inner surface was deformed by the earlier acceleration and coasting phases. The surface was perturbed by a sixth order Legendre polynomial summed over the laser beams. Figure 7 shows the inner surface at the end of the simulation. The pattern shows distinct spikes surrounded by valleys. However when the perturbation was inverted the opposite bubble was surrounded by a ridge. Hence the nature of the RT instability seems to be completely dependent on the initial conditions.

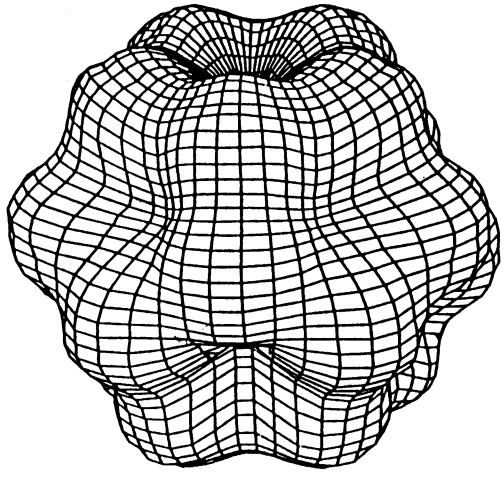

FIG. 7. The inner fuel–shell surface showing the spike–valley arrangement.

ACKNOWLEDGEMENTS

The authors thank the staff of the Central Laser Facility for their assistance and technical support.

REFERENCES

[1] WILLI, O., BASSETT, D., GIULIETTI, A., KARTTUNEN, S., Opt. Commun. **70** (1989) 487.
[2] COE, S., AFSHAR-RAD, T., WILLI, O., Opt. Commun. **73** (1989) 299.
[3] COE, S., AFSHAR-RAD, T., WILLI, O., Europhys. Lett. **11** (1990) 423.
[4] COE, S., AFSHAR-RAD, T., DESSELBERGER, M., KHATTAK, F., WILLI, O., GIULIETTI, A., LIN, Z.Q., YU, W., DANSON, C., Europhys. Lett **10** (1989) 31.
[5] WILLI, O., AFSHAR-RAD, T., COE, S., GIULIETTI, A., Phys. Fluids B **2** (1990) 1318.
[6] DANSON, C., BANN, R., PEPLER, D., RIZVI, N., ROSS, I., RUMSBY, P., JACKSON, R., COE, S., AFSHAR-RAD, T., DESSELBERGER, M., WILLI, O., Rep. RAL-89-045, Annual Report to the Laser Facility Committee 1989 (1989) 141.
[7] WILLI, O., RUMSBY, P., SARTANG, S., IEEE J. Quantum Electron. OE-17 (1981) 1909.
[8] WILLI, O., RUMSBY, P., HOOKER, C., RAVEN, A., LIN, Z., Opt. Commun. **41** (1982) 110.
[9] HAINES, M.G., Can. J. Phys. **64** (1986) 914.
[10] EDWARDS, J., BARROW, V., WILLI, O., ROSE, S., Europhys. Lett. **11** (1990) 631.
[11] DESSELBERGER, M., WILLI, O., SAVAGE, M., LAMB, M., submitted to Phys. Rev. Lett.
[12] GRUN, J., et al., Phys. Rev. Lett. **58** (1987) 2672.

DISCUSSION

H. TAKABE: With regard to the thermal instability driven by radiation cooling, have you checked, for example, the laser intensity dependence of the instability? As the emissivity and opacity of radiation are very sensitive to the plasma temperature, there should be a drastic change in different intensity ranges if the process is driven by radiation.

M.G. HAINES: These experimental results are very new, and we have not yet done a thorough theoretical comparison. However, the occurrence of the instability in the dense (10 $\times$ critical) region suggests that the thermal instability is driven by the return cold electron current associated with the heat flux in a region where the mean free path is less than the collisionless skin depth.